Supporting Information

Clinical Potential for Infected Wound Care: Synergistic Photothermal-Photodynamic Therapy Using a Conjugation-Bridge Modulated D-A-D Porous Organic Polymer

Jie Zheng,[a] Lei Ju,[a] Jie Sun,[a] Linlin Xu,[a] Junshan Zhang[b]*

a. *Department of Midwifery, Weifang Nursing Vocational College, Weifang 261041, China*

b. *Weifang People's Hospital, Shandong Second Medical University, Weifang, 261041, Shandong, PR China*

c. *Computer and Mathematics Teaching & Research Section, Weifang Nursing Vocational College, Weifang 261041, Shandong, PR China*

[#] These authors contribute equal to this work.

*Corresponding author.

E-mail: zhangjunshan_1@163.com

Contents

Section1. Synthesis Procedures

1.1 Materials

Triphenylamine, aluminum chloride ($AlCl_3$), dichloromethane (DCM), acetyl chloride, petroleum ether, Na_2SO_4, Pyrrole, 4-cyanobenzaldehyde, propanoic acid, methanol (MeOH), dicyandiamide, KOH, 2-methoxyethanol, dimethyl sulfoxide, and tetrahydrofuran (THF) were purchased from the commercial supplier and directly used without further purifications.

1.2 Synthesis of 4,4',4''-triacetyl Triphenylamine

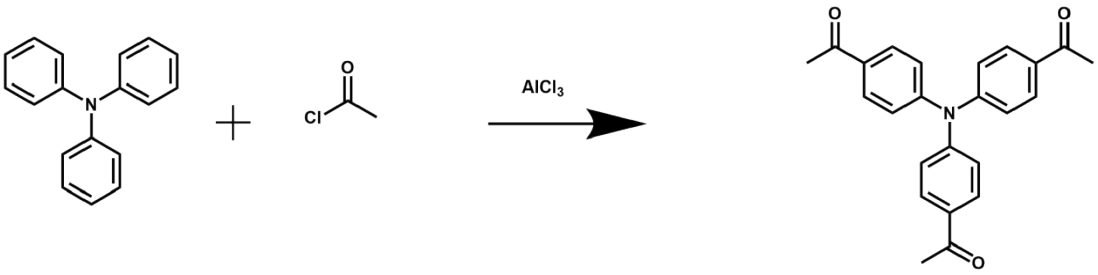

Triphenylamine (1.0 g, 4.1 mmol) and aluminum chloride1.8 g (13.5 mmol) were added to 150 ml of dry DCM. Then, acetyl chloride (2.0 ml, 28.28 mmol) was dissolved in 80 ml of dry DCM. The above two solutions were mixed which was stirred for 12 h at room temperature. Subsequently, 100 ml of distilled water was injected into the reaction system to quench the reaction. The aqueous layer was further extracted with CH_2Cl_2 (3×150 ml). The combined organic layers were dried by Na_2SO_4. The solution was concentrated under reduced pressure to give the crude product, which was purified by flash column chromatography on silica gel (V_{PE}: V_{CH2Cl2} =1: 10) to afford a cyan solid (0.7 g, 46.2%). ^1H NMR ($CDCl_3$, ppm): δ 7.90 (d, 6H), 7.15 (d, 6H), 2.58 (s, 9H).

1.3 Synthesis of 5,10,15,20-tetrakistetra(4-cyanophenyl) porphyrin

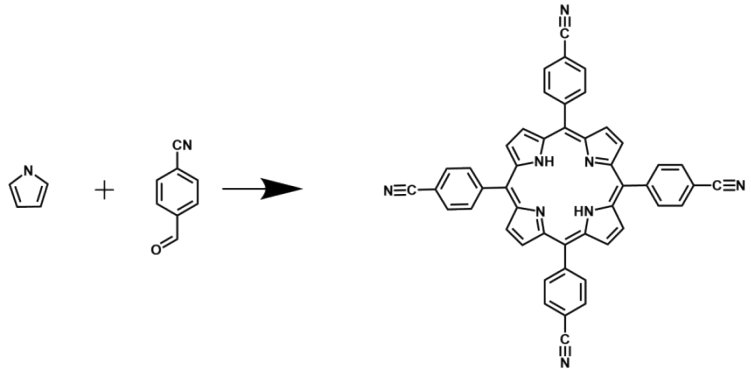

Pyrrole (3.52 mL, 50 mmol) and 4-cyanobenzaldehyde (5.0 g, 7 mmol) was added into a 500 mL round bottom flask containing 200 mL propionic acid. The reaction system was heated under reflux for 1 h. The reaction mixture was then cooled down to room temperature, following by the addition of 500 mL of MeOH. The reaction mixture was further stirred for 30 min in an ice bath. The resulting precipitate was filtered off and washed several times with MeOH until the filtrate was clear. Subsequently, the product was washed with 100 mL warm distilled water and dried at 70°C in a drying oven over night to yield the 5,10,15,20-tetrakistetra(4-cyanophenyl) porphyrin as purple-black solid (2.1g, 28%). ^{1}H-NMR: (500 MHz CDCl3): δ= 8.73 (s, 8H); 8.27 (d, 8H); 8.04 (d, 8H).

1.4 Synthesis of 5,10,15,20-tetrakis(4-(2,4-diaminotriazine) phenyl) porphyrin

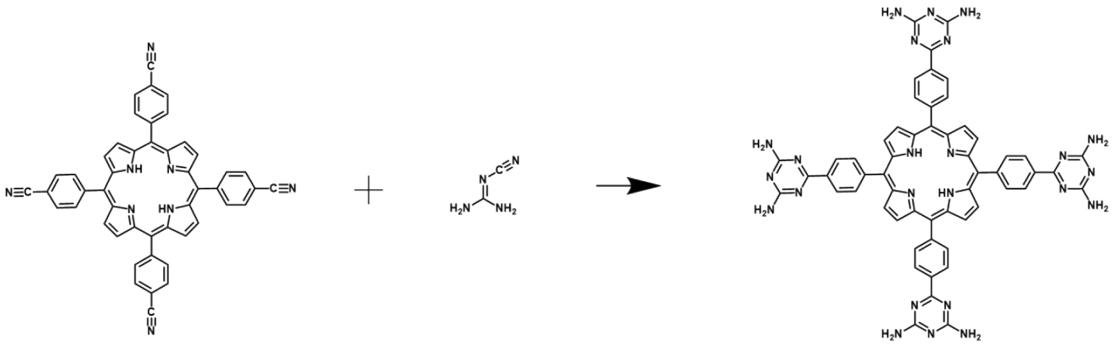

A mixture consisting of 5,10,15,20-tetrakis[tetra(4-cyanophenyl)]porphyrin (1.172 g, 1.64 mmol), dicyandiamide (0.79 g, 8.2 mmol), and KOH (0.6 g, 10.6 mmol) was dissolved in dry 2-methoxyethanol (40 mL). The solution was then heated under reflux for two days. The resulting precipitate was filtered and washed repeatedly with methanol until the filtrate became clear. Afterward, the product was washed with 150 mL of warm distilled water and dried overnight at 70 °C in a drying oven. This process yielded 0.65 g (32.2%) of 5,10,15,20-tetrakis(4-(2,4-diaminotriazine) phenyl)

porphyrin as a purple-black solid. The ^{1}H-NMR spectrum, recorded at 500 MHz in DMSO-d6, displayed signals at δ= 8.92 (s, 8H), 8.71 (d, 8H), 8.35 (d, 8H), and 6.89 (s, 16H).

1.5 Synthesis of Ac-COF

1.5.1 Synthesis of TPA-POR

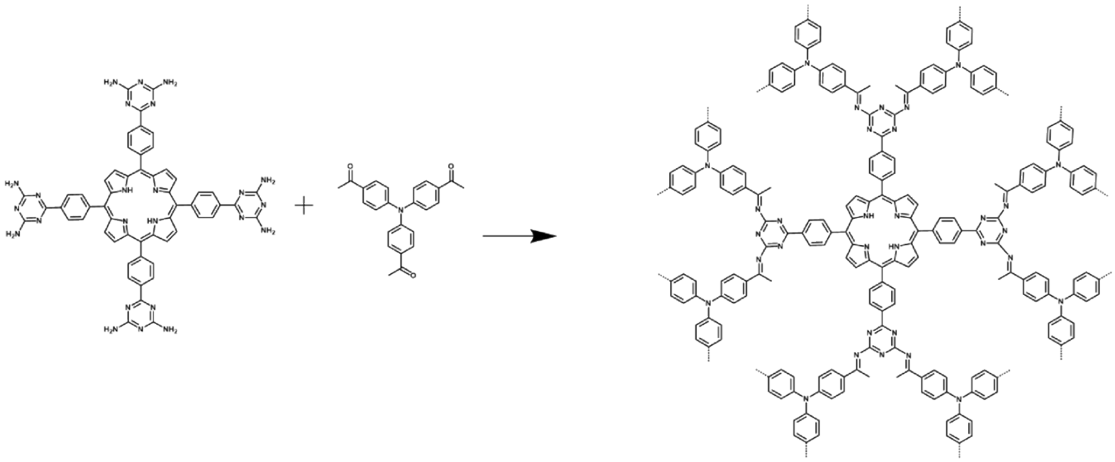

5,10,15,20-tetrakis[4-(2,4-diaminotriazinyl)phenyl]porphyrin (50 mg, 0.047 mmol) and 4,4',4''-triacetyltriphenylamine (47 mg, 0.126 mmol) were dissolved in 3 mL of dimethyl sulfoxide. Transfer the mixture to a high-pressure reactor, purge it with argon for 20 minutes, and then place it in an oven at 180 °C for 72 h (note that hydrogen sulfide gas will be generated, so handle with caution during post-processing). After cooling to room temperature, wash the filtrate with dichloromethane (DCM), methanol (MeOH), and tetrahydrofuran (THF) until the filtrate becomes colorless. Extract the residue by Soxhlet extraction with methanol and tetrahydrofuran for 12 hours each, and then dry it under vacuum at 80 °C for 12 hours to obtain 81 mg (83.5%) of a black powdery solid.

1.5.2 Synthesis of BP-POR, CB-POR, BE-POR

The remaining three polymers were synthesized following the identical procedure as TPA-POR, with the exception of utilizing acyl monomers with different structures. During the polymerizations, the dosage of the D-A structured 5,10,15,20-tetrakis(4-(2,4-diaminotriazinyl)phenyl)porphyrin remained constant at 50 mg (0.047 mmol).

For the synthesis of BP-POR, 4,4'-diacetylbiphenyl (45 mg, 0.19 mmol) was used, yielding a the final product as black solid (61 mg, yield 64.2%).

In the case of CB-POR, 1-(7-acetyl-9H-carbazol-2-yl)ethanone (47.8 mg, 0.19 mmol) was employed, resulting in the generation of final CMP as a brown, fluffy powder (73.2 mg, yield 74.8%).

Lastly, BE-POR obtained as black solid was prepared using the 1,4-diacetylbenzene (30.9 mg, 0.19 mmol) as the regulation agent. The final product was weight 57.1 mg (yield 70.6%).

Section 2. Methods

2.1 Photothermal Performance Test

Aqueous suspensions of TPA-POR, each with varying concentrations (0, 100, 200, 300, and 400 μg/mL), were individually dispensed into 1.5 mL EP tubes. Each sample was then irradiated with an 808 nm near-infrared laser at an intensity of 1.0 W·cm^-2 for a duration of 600 seconds. The temperature was meticulously recorded at intervals of 30 seconds using a thermal imaging camera. Furthermore, an additional experiment was conducted where a TPA-POR suspension with a concentration of 300 μg/mL was irradiated with an 808 nm near-infrared laser at varying intensities (0.5, 0.8, 1, 1.2, and 1.5 W·cm^{-2}) for 600 S. The temperature was again recorded every 30 S, and thermal images of the sample were captured at different time points. To assess the photothermal stability of TPA-POR, a heating/cooling cycle test was performed. The TPA-POR aqueous suspension (300 μg/mL) was irradiated with a near-infrared laser (808 nm, 1.0 W·cm^{-2}) for 10 minutes, followed by turning off the laser and allowing the suspension to cool to room temperature. This process was repeated for four cycles, and a curve was generated to evaluate the photothermal stability of TPA-POR.

2.1.1 Photothermic conversion efficiency (η).

$$\eta = \frac{hS\,(T_{max} - T_{max,\,water})}{I\,(1 - 10^{-A\lambda})} \qquad \text{(S1)}$$

Where, 'h' is the heat transfer coefficient. 'S' is the surface area of the container; 'T_{max}' is the equilibrium temperature after 10 min irradiation (T_{max}=58.9 °C); '$T_{max,\,water}$' is the temperature of the surrounding ($T_{max,\,water}$=22.2 °C); 'I' represents 808 nm laser power (1.0 W/cm^2) and 'A_{808}' is the absorbance of the ACOF-1 aqueous solution at 808 nm (A_{808}=0.74520). The value of 'hS' is determined according to equation (S2):

$$hS = \frac{m_d C_d}{\tau_S} \qquad \text{(S2)}$$

Where 'm_d' is the mass (1.0 g) and 'C_d' is the heat capacity (4.2 J/g) of the aqueous solvent; 'τ_S' is the sample system time constant and 'θ' is defined as the ratio of ΔT and ΔT_{Max}. The value of τ_S is determined according to equations (S3) and (S4):

$$\tau_S = -\frac{t}{ln\,\theta} \quad \text{(S3)}$$

$$\theta = \frac{T_{(t)} - T_{surr}}{T_{max} - T_{surr}} \quad \text{(S4)}$$

In this work, the The temperature rise is determined by:

$$\Delta T = T_{max} - T_{surr} = 58.9 - 22.2 = 36.7°C;$$

The fraction of absorbed laser energy is given by:

$$1 - 10^{-A_{808}} = 1 - 10^{-0.74520} \approx 1 - 0.1803 = 0.8197;$$

Thus, the absorbed power per unit area is:

$$I \times (1 - 10^{-A_{808}}) = 1.0\ W/cm^2 \times 0.8197 = 0.8197\ W/cm^2$$

The heat dissipation coefficient hS (Equation S2) was calculated as follows:

$$hS = \frac{m_d C_d}{\tau_S} = 1.0g \times 4.2\ J/g\ /\ 233.58s = 4.2\ J/233.58\ s \approx 0.01798\ W/°C$$

The Numerator of Equation S1

$$Numerator = hS \cdot \Delta T = 0.01798\ W/°C \times 36.7°C \approx 0.6599\ W$$

Compute the Denominator of Equation S1

$$Denominator = I \cdot (1\text{-}10^{-A_{808}}) = 1.0\ W/cm^2 \times 0.8197 \approx 0.8197\ W/cm^2$$

The denominator has units of W/cm^2, while the numerator is in W. This implies that the efficiency η is dimensionless when the laser irradiation area is consistent with the container surface area, as commonly assumed in such calculations.

Calculate the Photothermal Conversion Efficiency η (Using Equation S1)

$$H = Numerator/Denominator = 0.8197 W/cm^2 = 0.6599 W/0.8197\ W/cm^2 \approx 0.8047$$

Converting to a percentage:

$$\eta \approx 80.47\%$$

The time constant τs=233.58 s was derived from the linear fitting of the cooling curve in Figure 3h, which plots the negative natural logarithm of the temperature driving force versus time.

2.2 Assessment of Photodynamic performance test

To evaluate the overall photodynamic activity of the material, the generation of reactive oxygen species (ROS) was systematically investigated using a combination of direct spectroscopic detection and quantitative chemical probe assays under well-defined experimental conditions. All experiments were conducted under ambient conditions to enhance the clinical relevance and better simulate a natural treatment environment.

2.2.1. Direct Detection of ROS by Electron Paramagnetic Resonance (EPR) Spectroscopy

EPR spectroscopy with specific spin traps was employed as a direct method to identify paramagnetic ROS. Measurements were performed under both dark and 808 nm NIR laser irradiation (1.0 W/cm^2) conditions to confirm light-induced generation.

Singlet Oxygen ($^1O_2$, Type II Pathway)

To confirm oxygen-dependent $^1O_2$ generation, a solution of TPA-POR (20 μg mL^{-1}) and the spin trap 2,2,6,6-tetramethylpiperidine (TEMP, 50 mM) in acetonitrile (CH_3CN) was prepared and irradiated under ambient (normoxic) conditions. The characteristic 1:1:1 triplet signal of the stable TEMP-$^1O_2$ adduct was detected, indicative the formation of $^1O_2$ via the typical Type II Pathway.

Hydroxyl Radical (•OH, Type I Pathway)

To demonstrate oxygen-independent •OH generation, an aqueous solution of TPA-POR (20 μg mL^{-1}) containing the spin trap 5,5-dimethyl-1-pyrroline N-oxide (DMPO, 100 mM) was thoroughly purged with argon for 30 min to establish anoxic conditions prior to irradiation. Following irradiation, the EPR spectrum displayed the characteristic 1:2:2:1 quartet signal of the DMPO-•OH adduct which conclusively confirms the formation of hydroxyl radicals via a Type I pathway.

Superoxide Anion ($O_2^{\bullet-}$, Type I Pathway)

The generation of $O_2^{\bullet-}$ was assessed using DMPO (100 mM) in an acetonitrile solution containing TPA-POR (20 μg mL^{-1}). Upon irradiation, the formation of the DMPO-$O_2^{\bullet-}$ adduct was verified by its characteristic EPR spectrum, exhibiting a primary spectral pattern, which is diagnostic for superoxide anion generation through

the typical type I Pathway.

2.2.2. Quantification of ROS Generation by Chemical Probe Assays

Complementary colorimetric and fluorescence assays using specific chemical probes were conducted to quantify ROS yields.

Singlet Oxygen ($^1O_2$, Type II Pathway)

The probe 1,3-diphenylisobenzofuran (DPBF, 20 μM) was used. $^1O_2$ oxidizes DPBF, decreasing its absorbance at 410 nm. The absorbance decay of a DPBF solution containing TPA-POR (10 μg mL^{-1}) was monitored under NIR irradiation (808 nm, 1.0 W/cm^2) at intervals (0, 1, 3, 6, 10 min). Control experiments with DPBF alone confirmed probe stability.

Hydroxyl Radical (•OH)

Methylene blue (MB, 10 μg mL^{-1}) degradation was used as an indicator. An aqueous MB solution containing TPA-POR (15 μg mL^{-1}) was deoxygenated by argon purging for 20 min. The absorbance at 664 nm was monitored before and after NIR irradiation (0, 2, 4, 6, 8, 10 min). A significant reduction in absorbance (>60%) under irradiated, anoxic conditions confirmed robust •OH production.

Superoxide Anion ($O_2^{\bullet-}$)

The fluorescence probe dihydrorhodamine 123 (DHR123, 5 μM) was utilized. $O_2^{\bullet-}$ oxidizes non-fluorescent DHR123 to fluorescent rhodamine 123 (λex/λem = 500/536 nm). The fluorescence intensity of a solution containing TPA-POR (10 μg mL^{-1}) and DHR123 was recorded under NIR irradiation at specified intervals (0, 2, 4, 6, 8, 10 min), with DHR123 alone serving as a control.

Total ROS:

The general ROS-sensitive fluorescent probe 2',7'-dichlorodihydrofluorescein (DCFH) was used. The fluorescence intensity of a mixture of TPA-POR and DCFH was measured every 2 min during 10 min of NIR irradiation (808 nm, 1.0 W/cm^2).

2.2.3. Summary of Photodynamic Mechanism

The combination of direct EPR detection and quantitative probe assays provides comprehensive evidence that TPA-POR generates ROS via both Type I and Type II pathways. The key advantage for potential application in hypoxic environments stems

from its confirmed Type I activity. The donor-acceptor-donor (D-A-D) structure of TPA-POR promotes efficient charge separation upon photoexcitation, enabling direct electron transfer to substrates to generate radicals such as •OH independently of molecular oxygen.

2.3 Stability test and long-term performance

To study the stability of TPA-POR, we prepared TPA-POR complexes (300 μg/mL) at the same concentration. The UV absorption intensity of TPA-POR solution at 808 nm was measured at different pH levels (pH = 1.5, 2.5, 3.5, 4.5, 5.5, 6.5, 7.5).

TPA-POR solution (300 μg/mL) was irradiated with 1.0 W/cm 808 nm infrared light for four cycles of laser on/off. The temperatures of four cycles were recorded, as shown in Fig. 4d. Meanwhile, after four laser on/off cycle irradiation experiments, we detected the UV absorption spectrum of TPA-POR.

In addition, we further investigated the stability of TPA-POR solution. We kept the TPA-POR solution for different times (0, 5, 10 and 15 days) and the changes in its UV absorption were studied.

2.4 Antibacterial performance test

The antibacterial efficacy of TPA-POR was evaluated against Gram-positive Staphylococcus aureus (S. aureus) and Gram-negative Escherichia coli (E. coli). Bacteria were cultured to mid-log phase, harvested by centrifugation, washed with phosphate-buffered saline (PBS, pH 7.4), and resuspended to a final concentration of 1×10^8 colony-forming units per milliliter (CFU/mL).

For the photodynamic/photothermal treatment, 50 μL of bacterial suspension was mixed with varying volumes (0, 25, 50, 75, 100, 150 μL) of a TPA-POR stock solution (2 mg/mL) in 1.5 mL microcentrifuge tubes. Sterile PBS was added to each tube to adjust the total volume to 1 mL, yielding final TPA-POR concentrations of 0, 50, 100, 150, 200, and 300 μg/mL, respectively. The mixtures were then irradiated with an 808 nm near-infrared (NIR) laser at a power density of 1.0 $W \cdot cm^{-2}$ for 10 min. Control groups included bacteria treated with TPA-POR in the dark and bacteria irradiated without TPA-POR.

Following treatment, 100 μL of each mixture was spread evenly on solid lysogeny broth (LB) agar plates and incubated at 37 °C for 24 h for qualitative colony observation. For quantitative analysis, the treated bacterial suspensions were serially diluted in PBS, plated on LB agar, incubated overnight, and viable colonies were counted. Antibacterial activity was expressed as the percentage reduction in CFU/mL relative to the PBS-treated control. All experiments were performed in three independent biological replicates.

2.5 Bacterial live/dead staining

The membrane integrity of bacteria following treatment was assessed using the LIVE/DEAD™ BacLight™ bacterial viability kit. S. aureus and E. coli suspensions were treated with TPA-POR with or without NIR irradiation as described in Section 2.4. After treatment, bacterial pellets were collected, resuspended in a staining solution containing a mixture of SYTO 9 and propidium iodide (PI), and incubated in the dark for 20 minutes at room temperature. SYTO 9 stains all bacteria green, while PI only penetrates bacteria with compromised membranes, staining them red. The stained samples were then imaged using an inverted fluorescence microscope.

2.6 Cytotoxicity Evaluation (MTT assay)

The cytotoxicity of TPA-POR towards mammalian cells was evaluated using the 3-(4,5-dimethylthiazol-2-yl)-2,5-diphenyltetrazolium bromide (MTT) assay on human embryonic kidney (HEK293) and human normal liver (HL7702) cell lines.

Cells were seeded in 96-well plates at a density of 5×10^3 cells per well in 100 μL of complete culture medium. The outer perimeter wells were filled with 200 μL of PBS to minimize evaporation. After 24 h of incubation to allow cell attachment, the medium was replaced with fresh medium containing TPA-POR at a range of final concentrations (0, 100, 200, 300, 400, 500 μg/mL). Two treatment regimes were applied: a “Light” group exposed to NIR irradiation (808 nm, 1.0 $W \cdot cm^{-2}$, 10 min) immediately after adding TPA-POR, and a “Dark” group kept in the dark. Cells were then incubated for an additional 24 h

Subsequently, 10 μL of MTT solution (5 mg/mL in PBS) was added to each well,

and the plates were incubated for 4 hours at 37 °C. The formazan crystals formed were dissolved by adding 100 µL of dimethyl sulfoxide (DMSO) to each well after careful removal of the supernatant. The absorbance of the solution was measured at 490 nm using a microplate reader. Cell viability was calculated as a percentage relative to the untreated control cells. Data are presented as the mean ± standard deviation (SD) from three independent experiments, each with six technical replicates (n=3).

2.7 Hemolysis test of materials

Fresh blood was obtained from KM female mice. Red blood cells (RBC) were collected, centrifuged at 1500 rpm for 20 min, and then washed with PBS until the supernatant was colorless. The supernatant was discarded and the erythrocytes were mixed with an appropriate amount of PBS and carefully blown up. Erythrocyte to PBS ratio of 3:11 (v:v). RBCs were then incubated with (100 ~ 500µg/mL) of, TPA-POR at a ratio of 1:9 (v/v) for 3 h at 37 °C, followed by centrifugation at 12,000 rpm for 20 min. Then, it was measured by UV-Vis spectroscopy at 540 nm. Distilled water was used as a positive control and PBS as a negative control. Hemolysis was calculated using the formula:

$$Hemolysis\ (\%) = \frac{A_s - A_n}{A_p - A_n} \times 100\%$$

A_s: Absorbance of TPA-POR group.

A_n: Absorbance of the PBS group (negative control).

A_p: Absorbance of the Water group (positive control).

2.8 Data Analysis

Results are expressed as mean ± SD of three independent replicate experiments. Statistical significance was assessed using Student's two-tailed t-test, with *P < 0.05, **P < 0.01, and ***P < 0.001 considered significant.

Section 3. FT-IR Spectroscopy

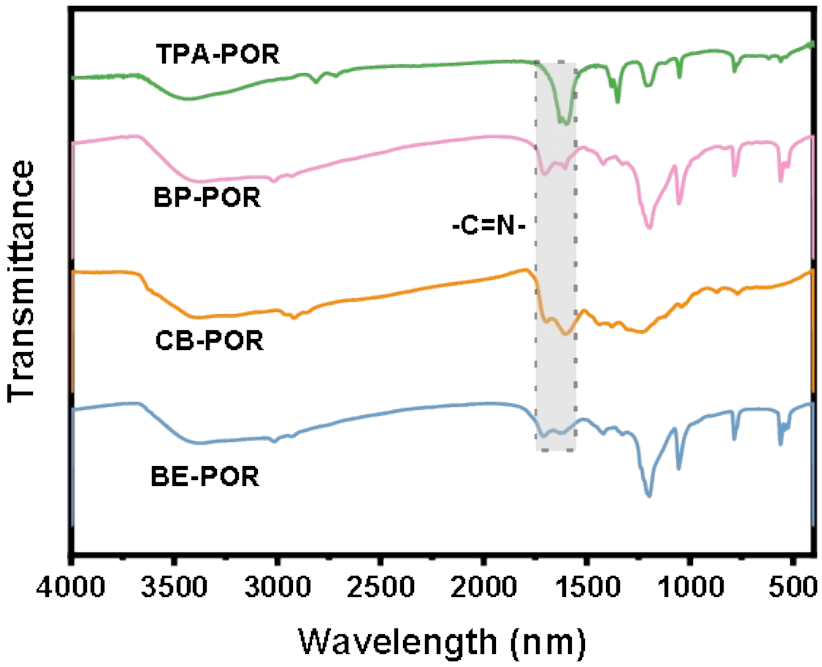

Figure S1. FT-IR Spectroscopy of TPA-POR, BP-POR, CB-POR and BE-POR polymers.

Section 4. XPS, XRD and TG of TPA-POR

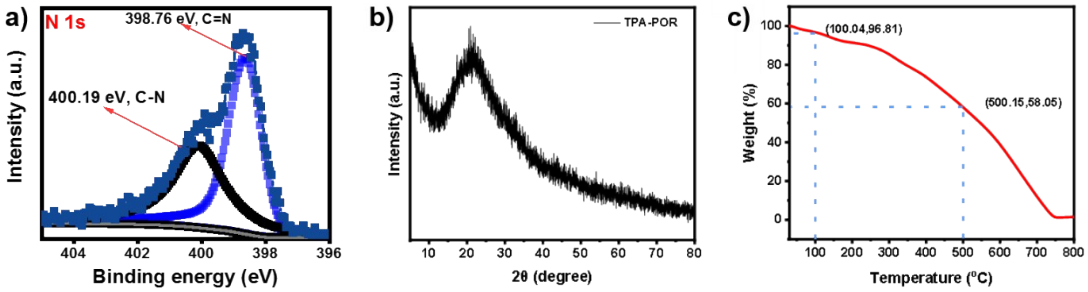

Figure S2. a) High resolution XPS N 1s spectrum of TPA-POR; b) Powder XRD of TPA-POR; c) Weight variation of TPA-POR with increasing temperature in a nitrogen atmosphere.

Section 5. EDS and elemental content from TEM mapping

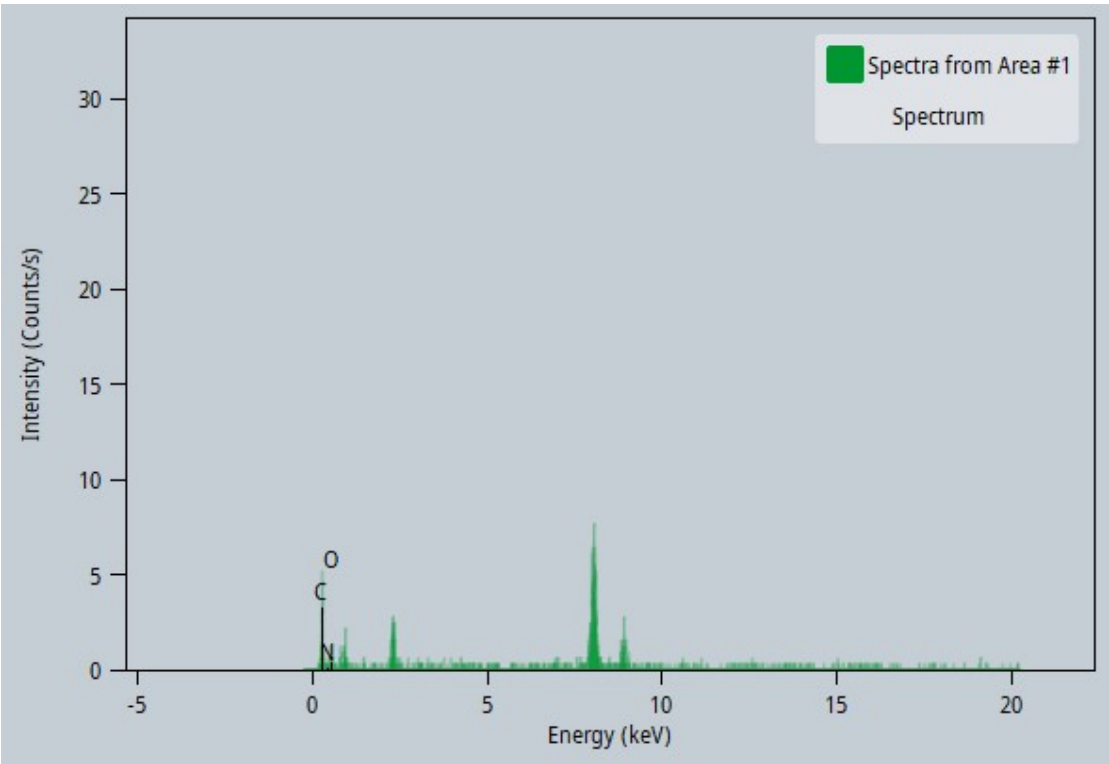

Figure S3. EDS and elemental content from TEM mapping.

Section 6. TEM of BP-POR, CB-POR and BE-POR

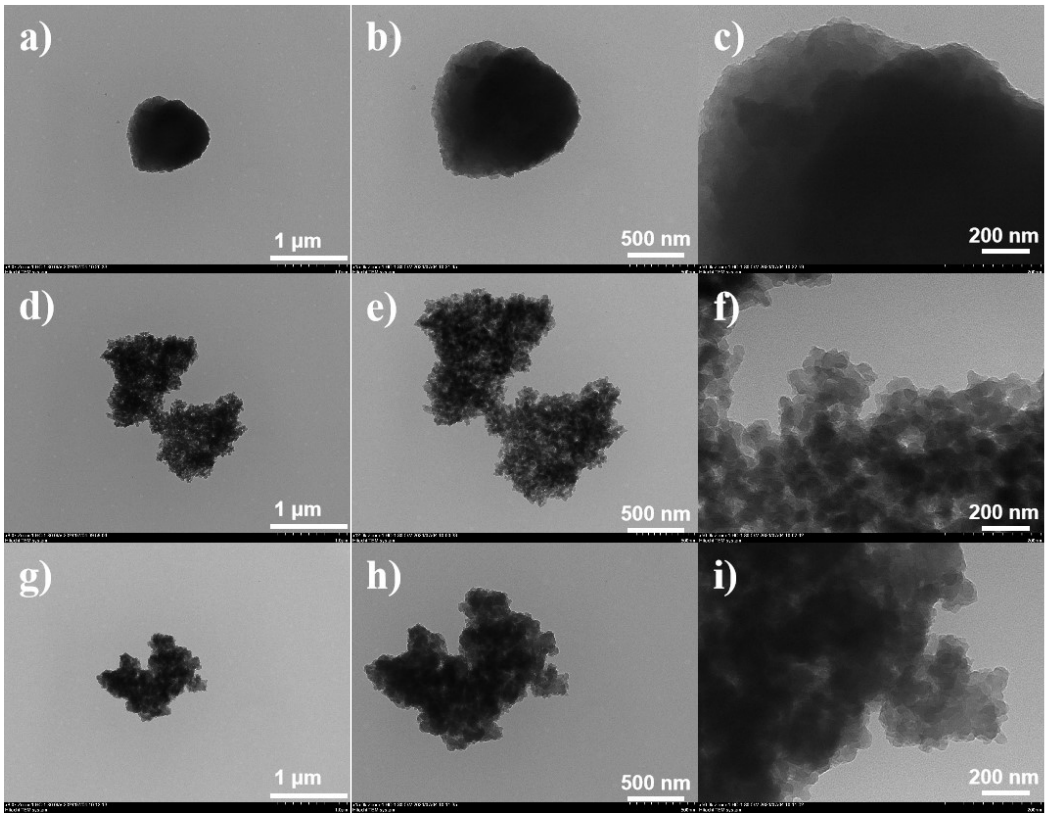

Figure S4. TEM images of BP-POR (a-c) at different magnifications, respectively; TEM images of CB-POR (d-f) at different magnifications, respectively; TEM images of BE-POR (g-i) at different magnifications, respectively.

Section 7. Stability experiments with TPA-POR

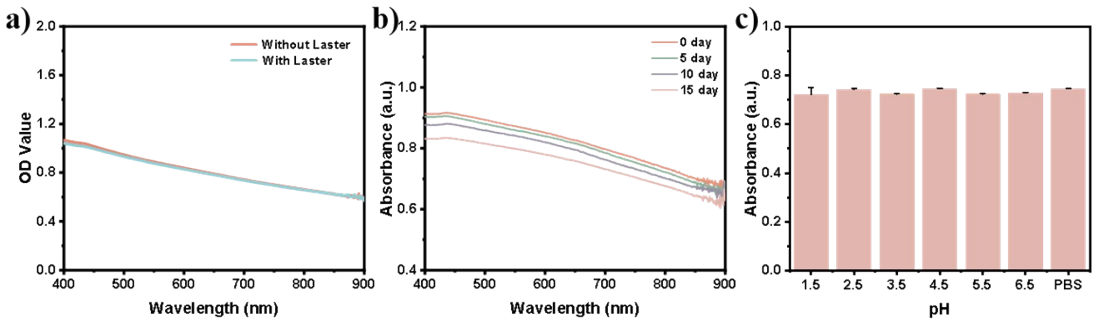

Figure S5. a) UV absorption curves of materials before and after photothermal cycling; b) Changes in UV absorption of TPA-POR after storage in water for different periods of time (0, 5, 10, and 15 day); c) The absorbance values of TPA-POR at different pH levels.

Section 8. Total photodynamic effect of TPA-POR

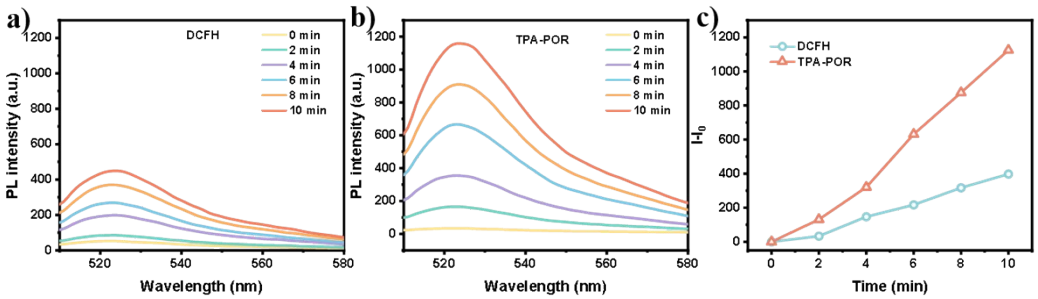

Figure S6. a) DCFH Changes in fluorescence of probes in the presence of laser (808nm, 1.0 W/cm$^{2)}$; b) Changes in fluorescence intensity of probes under laser irradiation after addition of TPA-POR; c) Comparison of the decay rate of DCFH induced by TPA-POR under 808 nm laser irradiation.

Section 9. TPA-POR antimicrobial at different concentrations

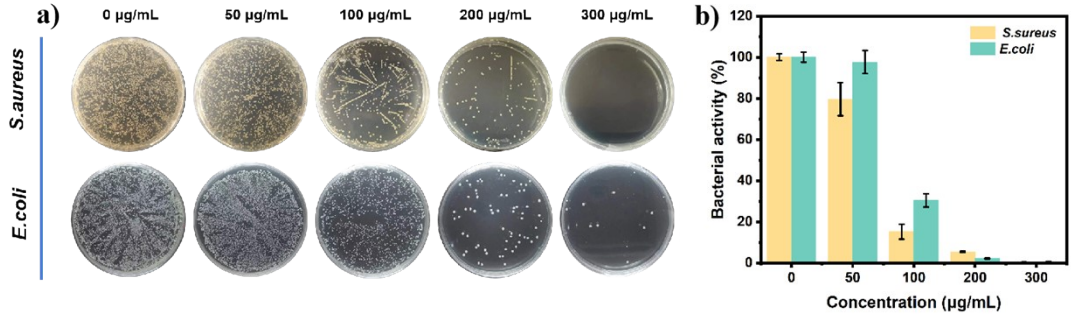

Figure S7. a) Results of bacterial plate coating after treatment with different concentrations of TPA-POR; b) Quantification of bacterial smears by plate counting.

Section 10. Cell scratching assay

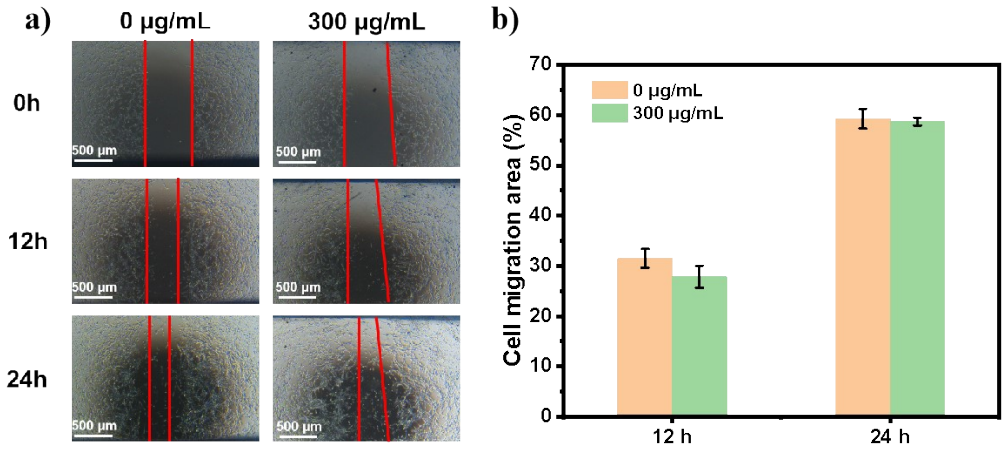

Figure S8. a) Cell migration experiments of TPA-POR materials. a; b) Remaining migrated area of cell scratch after time in each group.

Section 11. Mouse Wound Temperature Detection

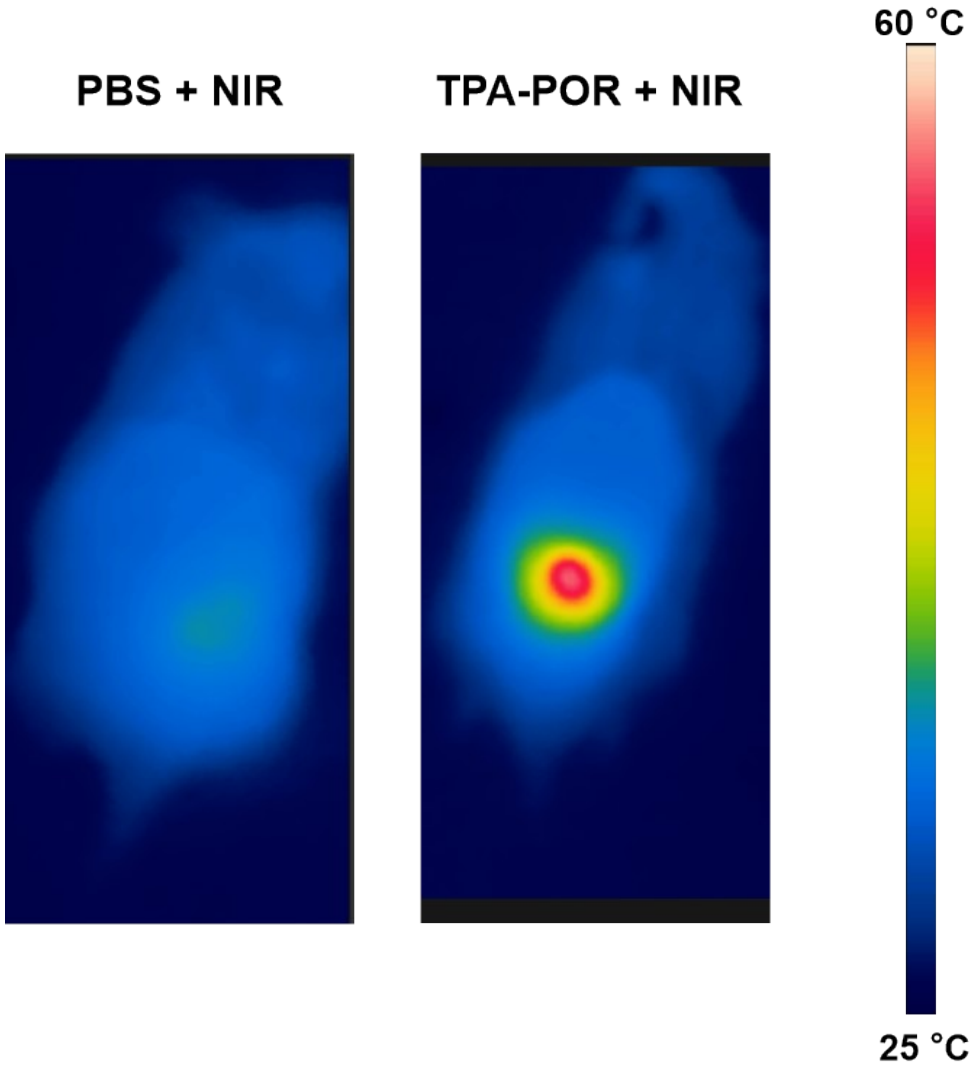

Figure S9. Temperature at the wound after laser irradiation in the PBS + NIR group and the TPA-POR + NIR group.

Section 12. Hematological examination

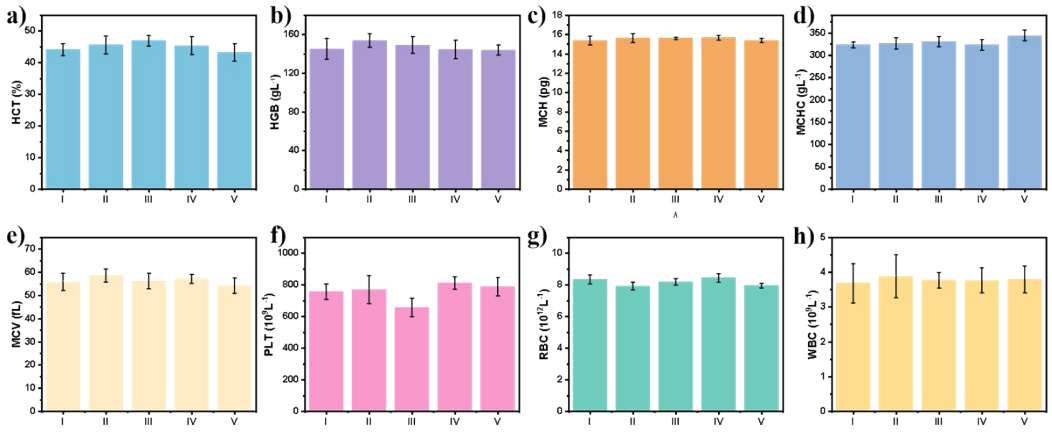

Figure S10. Hematological examination results (HCT, HGB, MCH, MCHC, MCV, PLT, RBC and WBC) of the corresponding group (day 8). Mean ± standard error data (n=3) were used.(I: blank group, II: PBS group, III: PBS + NIR group, IV: TPA-POR group, V: TPA-POR + NIR group).

Section 13. Supporting Tables

Table S1. Polymers -based antibacterial agent

	Power Density (W/cm^2)	Laser Wavelength (nm)	PCE (%)	Reference
TPA-POR	**1.0**	**808**	**80%**	**This work**
TAQ NPs	**0.8**	**808**	**79.7%**	**[1]**
FAQ NPs	**0.8**	**808**	**72.0%**	**[1]**
Zr-Fc MOF	**1.0**	**808**	**53%**	**[2]**
PEG @ Zr-Fc MOF	**2.0**	**808**	**46%**	**[3]**
PDA-Pt-CD @ Ru Fc NPs	**1.0**	**808**	**44.5%**	**[4]**
Cu-Fc	**1.0**	**808**	**38.4%**	**[5]**
CG/PDA @ Ag	**1.0**	**808**	**38.2%**	**[6]**
Fe_3O_4-CB@Au-Fc NPs(Au : Fe=1:2)	**1.0**	**808**	**36.7%**	**[7]**
FA-CNPs	**1.0**	**808**	**36.5%**	**[8]**
MSN @ Au-Fc	**2.0**	**808**	**35.9%**	**[9]**
Fc-HP°/HD/GOx	**1.0**	**808**	**35.6%**	**[10]**
PDA NPs	**1.6**	**808**	**32%**	**[11]**
CuS NPs	**1.0**	**808**	**28.51%**	**[12]**

CuS aggregates	**1.0**	**808**	**28.43%**	**[12]**
ferrocene-based polymer	**2.0**	**808**	**19.25%**	**[13]**
ID@MOS-Fc-CDHA	**1.0**	**808**	**18.6%**	**[14]**
COi6-4Cl	**0.3**	**808**	**13.4**	**[15]**

Section 14. Supporting References

[1] X. Yang, L. Wen, G. Xu, H. Lin, S. Wang and J. Liu, *Bioorg. Chem.,* 2023, **130**, 106220.

[2] Z. Deng, C. Fang, X. Ma, X. Li, Y.J. Zeng and X. Peng, *ACS Appl. Mater. Interfaces,* 2020, **12**, 20321-20330.

[3] X. Wang, X. Sun, T. Bu, Q. Wang, H. Zhang, P. Jia, L. Li and L. Wang, *Acta. Biomater.,* 2021, **135**, 342-355.

[4] J.H. Liang, Y. Zheng, X.W. Wu, C.P. Tan, L.N. Ji and Z.W. Mao, *Adv. Sci.*, 2020, **7**, 1901992.

[5] J. Yang, L. Yang, Q. Li and L. Zhang, *J. Colloid. Interface Sci.,* 2022, **626**, 719-728.

[6] X. Qi, Y. Huang, S. You, Y. Xiang, E. Cai, R. Mao, W. Pan, X. Tong, W. Dong, F. Ye and J. Shen, *Adv. Sci.*, 2022, **9**, 2106015.

[7] Q. Cheng, L. Yue, J. Li, C. Gao, Y. Ding, C. Sun, M. Xu, Z. Yuan and R. Wang, *Small.,* 2021*,* **17**, e2101332.

[8] Z. He, L. Zhao, Q. Zhang, M. Chang, C. Li, H. Zhang, Y. Lu and Y. Chen. *Adv. Fun. Mater.,* 2020, **30,** 1910301.

[9] Y. Bai, J. Wu, K. Liu, X. Wang, Q. Shang and H. Zhang, *J. Colloid. Interface Sci.,* 2023, **637**, 399-407.

[10] S.Y. Lee, J. Park, D.I. Jeong, C. Hwang, J. Lee, K. Lee, H.J. Kim and H.J. Cho, *J. Control. Release.,* 2022, **349**, 617-633.

[11] Y. Zhang, K. Zhang, H. Yang, Y. Hao, J. Zhang, W. Zhao, S. Zhang, S. Ma and C. Mao, *ACS Appl. Mater. Interfaces,* 2023, **15**, 14099–14110.

[12] J. Li, Q. Cheng, L. Yue, C. Gao, J. Wei, Y. Ding, Y. Wang, Y. Zheng and R. Wang, *Nanoscale Horiz*., 2021, **6**, 907-912.

[13] W. Zhu, C. Zhang, Y. Chen and Q. Deng, *Polymers,* 2021, **13**, 558.

[14] H. W. Choi, J. H. Lim, T Kang, and B. G. Chung, *Antioxidants*, 2022, **11**, 2137.

[15] L. Li, C. Shao, T. Liu, Z. Chao, H. Chen, F. Xiao, H. He, Z. Wei, Y. Zhu, H. Wang, X. Zhang, Y. Wen, B. Yang, F. He and L. Tian, (2020). *Adv. Mater.,* 2020, **32**, 2003471.